

Estuarine salinity response to freshwater pulses

Bouke Biemond¹, Huib E. de Swart¹, Henk A. Dijkstra¹, Manuel
Díez-Minguito²

¹Institute for Marine and Atmospheric research Utrecht, Department of Physics, Utrecht University,
Utrecht, the Netherlands.

²Environmental Fluid Dynamics Group, Andalusian Institute for Earth System Research, University of
Granada, Granada, Spain

Key Points:

- Modeling of salt dynamics during strong freshwater pulses requires a detailed description of the vertical structure of salinity.
- Dependence of salt intrusion length is quantified from the pulse duration and ratio of river discharge before and during a pulse.
- The recovery time after a freshwater pulse does not depend on the change in salt intrusion length induced by the pulse.

Corresponding author: Bouke Biemond, w.t.biemond@uu.nl

Abstract

Freshwater pulses (during which river discharge is much higher than average) occur in many estuaries, and strongly impact estuarine functioning. To gain insight into the estuarine salinity response to freshwater pulses, an idealized model is presented. With respect to earlier models on the spatio-temporal behavior of salinity in estuaries, it includes additional processes that provide a more detailed vertical structure of salinity. Simulation of an observed salinity response to a freshwater pulse in the Guadalquivir Estuary (Spain) shows that this is important to adequately simulate the salinity structure. The model is used to determine the dependency of the estuarine salinity response to freshwater pulses for different background discharge, tides and different intensities and durations of the pulses. Results indicate that the change in salt intrusion length due to a freshwater pulse is proportional to the ratio between peak and background river discharge and depends linearly on the duration of the pulse if there is no equilibration during the pulse. The adjustment time, which is the time it takes for the estuary to reach equilibrium after an increase in river discharge, scales with the ratio of the change in salt intrusion length and the peak river discharge. The recovery time, i.e. the time it takes for the estuary to reach equilibrium after a decrease in river discharge, does not depend on the amount of decrease in salt intrusion length caused by the pulse. The strength of the tides is of minor importance to the salt dynamics during and after the pulse.

Plain Language Summary

The salinity distribution in an estuary, the transition area between river and sea, strongly depends on the river discharge. During periods of low river discharge, salt will move upstream, but when river discharge becomes high, salt is pushed downstream. This study focuses on the effect of freshwater pulses (short periods with sudden high river discharge) on estuarine salt intrusion. When applying an existing model to observed freshwater pulses in the Guadalquivir Estuary (Spain), it turned out that this model was not able to simulate the effect of strong pulses. A new model has been developed that performs well when being applied to the same situations. With this new model, it is shown that the intensity and duration of the pulse control the decrease in salt intrusion. The strength of the tides is found to be of minor importance. The time it takes before the salt intrusion has recovered to its initial location is determined by the river discharge after the pulse and does not depend on how much the salt intrusion moved downstream.

1 Introduction

Freshwater pulses, during which the freshwater discharge by rivers exceeds three times its long-yearly average value and which last no longer than one month, are common features in many estuaries around the world. They are mostly the result of strong precipitation in the upstream river catchment area (Tee & Lim, 1987; Valle-Levinson et al., 2002; Gong et al., 2007; Liu et al., 2008; Du & Park, 2019; Du et al., 2019; Guerra-Chanis et al., 2021), opening of a freshwater reservoir (Ingram et al., 1986; Lepage & Ingram, 1988), or a combination of those two (Díez-Minguito et al., 2013). The increased freshwater discharge causes a strong downstream transport of salt, which has a large impact on the ecology in the estuary and on the agriculture of the lands around the estuary (Paerl et al., 2006; McFarland et al., 2022). All the above-cited studies indicate that the adjustment time, here defined as the time during which the salinity in an estuary adjusts to high river discharge, is in the order of 1-2 days. Observational studies report that freshwater pulses can cause the salt intrusion length, which is defined as the distance of the 2 psu isohaline to the estuary mouth (Monismith et al., 2002), to shift by tens of kilometers (Díez-Minguito et al., 2013). An estuary can even become entirely fresh (Du & Park, 2019). After such pulses, the estuary returns to its non-disturbed state. Values of the recovery time, defined as the time it takes for the salt intrusion length to reach

65 its background value again, widely vary, but typically they are considerably larger than
66 values of the preceding adjustment times. For example, Valle-Levinson et al. (2002) found
67 10 days for the Chesapeake Bay (USA), whilst Gong et al. (2007) reported four months
68 for York River estuary, which is located in the same area.

69 The overall aim of this study is to gain a more detailed understanding of how an
70 estuary will respond to freshwater pulses with different intensity and duration. For such
71 purposes, it is helpful to employ idealized models, which only represent the most dom-
72 inant physical processes and assume a simplified geometry. Besides yielding insight into
73 the dynamics, these models are fast, flexible and are thus suitable for extensive sensi-
74 tivity analysis. Earlier studies on estuarine physics (Hansen and Rattray (1965); Chatwin
75 (1976); MacCready (2004); Geyer and MacCready (2014)) have demonstrated the added
76 value of idealized models with respect to detailed numerical models.

77 The current knowledge of estuarine adjustment to changes in river discharge origi-
78 nates from both simplified and more sophisticated numerical models. Kranenburg (1986)
79 demonstrated, by using analytical arguments applied to a one-dimensional model, that
80 the response timescale, i.e. the time during which an estuary responds to a decrease or
81 increase in river discharge, is inversely proportional to the river discharge after the change.
82 This finding explains the difference between adjustment time and recovery time. Hetland
83 and Geyer (2004) used a three-dimensional primitive equation model with idealized ge-
84 ometry and simple turbulence formulations to study response timescales. They found
85 a clear difference between adjustment and recovery time, which is in line with the find-
86 ing of Kranenburg (1986). They argued that during net upstream transport of salt, the
87 motion of the salt intrusion adds constructively to the (subtidal) bottom layer flow. This
88 means that velocities in the bottom layer are stronger than during net downstream trans-
89 port, so import of salt will experience stronger resistance from the bottom drag and will
90 thus be slower than net export of salt. Chen (2015) extended the analysis of Kranenburg
91 (1986) by allowing the density-driven flow in his model to be time-dependent. He argued
92 that the difference between adjustment and recovery time is the result of the non-linear
93 response of salt intrusion length to changes in river discharge. Monismith (2017) employed
94 a modified version of the model of Chen (2015) to study the unsteadiness of the salt in-
95 trusion length under different time-dependent forcings. His model showed good skill in
96 hindcasting salt-intrusion lengths in the northern part of San Francisco Bay.

97 These studies yielded important insights into the timescales associated with the re-
98 sponse of salt intrusion to changes in river discharge. Important to mention here is that
99 the idealized models for estuarine adjustment assume that creation of salinity stratifi-
100 cation by vertically-sheared velocity is balanced by destruction of stratification by ver-
101 tical mixing. This assumption is based on Pritchard (1954), who analyzed observations
102 in the James River estuary under relatively low river discharge. Hereafter, we will re-
103 fer to this balance of processes determining the stratification as the Pritchard balance.
104 Studies by MacCready (2007) and Ralston et al. (2008) demonstrated that this assump-
105 tion works quite well in cases that they consider, but these cases do not include strong
106 freshwater pulses. Dijkstra and Schuttelaars (2021) showed that in steady state the Pritchard
107 balance does not hold in the high-discharge regime. It may be expected that this is also
108 true for time-dependent cases. Knowledge gaps also exist with regard to the sensitivity
109 of the response of the estuary to freshwater pulses for different environmental settings,
110 e.g. different strengths of tides.

111 The specific aims of this study are twofold. The first is to show the limitations of
112 the Pritchard balance when investigating strong freshwater pulses. The second is to in-
113 vestigate the sensitivity of the estuarine salinity response to a freshwater pulse to dif-
114 ferent parameters. We quantify the estuarine salinity response by calculating adjustment
115 timescales, recovery timescales and changes in salt intrusion lengths. There are three re-
116 search questions associated with this second aim: 1) What is the effect of the background
117 conditions of the estuary, i.e. the background river discharge and the strength of the tides,

118 on the salinity response? 2) What is the effect of the strength of the peak river discharge
 119 on the salinity response? 3) What is the effect of the duration of the pulse on the salin-
 120 ity response?

121 The remaining of this paper is organized as follows: In Section 2.1, deficiencies, in-
 122 cluding negative salinity values, are identified when the model of MacCready (2007) (MC07
 123 hereafter), which uses the Pritchard balance, is forced with observed river discharge dur-
 124 ing a strong freshwater pulse in the Guadalquivir Estuary (Spain). A new model, which
 125 does not rely on the Pritchard balance, is presented in Section 2.2. This model does not
 126 have the deficiencies of MC07 when used to simulate freshwater pulses in the Guadalquivir
 127 Estuary (Section 2.3). Afterwards, a sensitivity analysis is done in a more idealized model
 128 setup. The experimental setup is given in Section 2.4, followed by the results and dis-
 129 cussion (Section 3) and the conclusions (Section 4).

130 2 Material and Methods

131 2.1 Limitations of the Pritchard balance

132 In order to show the limitations of available idealized models for estuarine adjust-
 133 ment, the MC07 model is used to simulate the estuarine response to an observed strong
 134 freshwater pulse. This model simulates time-dependent, tidally averaged, width-averaged
 135 estuarine flow and salinity, building on Hansen and Rattray (1965). The vertical momen-
 136 tum balance is hydrostatic, while in the horizontal a balance is assumed between the pres-
 137 sure gradient force and internal friction. Furthermore, the Pritchard balance is used to
 138 describe the vertical structure of salinity. The MC07 model is here applied to the fresh-
 139 water pulse in February 2009 in the Guadalquivir estuary (Díez-Minguito et al., 2013;
 140 Wang et al., 2014; Losada et al., 2017). This pulse has a maximum discharge (main river
 141 + tributaries) of $889 \text{ m}^3 \text{ s}^{-1}$, while the river discharge in the month before the pulse has
 142 an average value of about $32.3 \text{ m}^3 \text{ s}^{-1}$. The model settings are as follows: the estuary
 143 is 110 km long and its width increases exponentially from 150 m at the upstream limit
 144 to 650 m at the mouth. The thalweg has an average depth of 7.1 m (Díez-Minguito et
 145 al., 2013), so this is used as the depth of the estuary. The vertical eddy-viscosity coef-
 146 ficient, vertical eddy-diffusion coefficient and horizontal eddy-diffusion coefficient are cho-
 147 sen as in Guha and Lawrence (2013). This means that they depend on the strength of
 148 the tidal current and a turbulent length scale, which is the estuary depth for the verti-
 149 cal coefficients and the estuary width for the horizontal coefficient. The model is forced
 150 with the observed river discharge from the Alcalá del Río dam and from the four main
 151 tributaries after this dam: Aznalcázar, El Gergal, Guadaíra and the Torre del Águila (Agen-
 152 cia de Medio Ambiente y Agua de Andalucía, see chguadalquivir.es/saih/Inicio.aspx).
 153 The representative tidal current amplitude is based on measurements (Navarro et al.,
 154 2011) and set to be 1.15 m s^{-1} and the ocean salinity is 35 psu. The horizontal grid size
 155 is 250 m and a timestep of 15 seconds is used to ensure numerical stability.

156 Results from this simulation are displayed in Fig. 1a and b. Before the pulse, the
 157 salinity field is only slightly disturbed by the variations in river discharge. During the
 158 freshwater pulse, surface salinity values drop and within a few days after the start of the
 159 pulse they reach values of -4.7 psu close to the mouth. The minimum value for surface
 160 salinity is thus below zero. Note that at the same time, bottom salinity values at the es-
 161 tuary mouth are prescribed to be 35 psu, which means that the estuary is strongly strat-
 162 ified during the pulse in this simulation. After the pulse, negative salinity values disap-
 163 pear. Salt intrusion recovers in about three weeks to values comparable to the ones be-
 164 fore the pulse. The negative values of surface salinity during the pulse are unphysical
 165 and motivated the development of a new model that is presented in the next section.

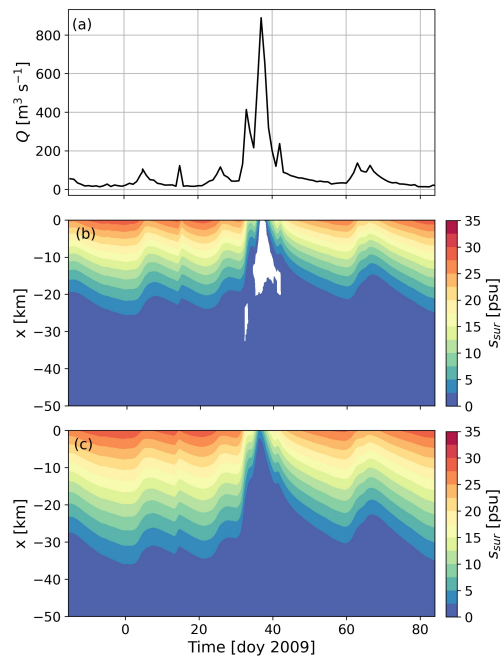


Figure 1. Application of two different models for the case of an observed freshwater pulse in the Guadalquivir Estuary in February 2009. (a) Time series of observed river discharge. (b) Simulated surface salinity s_{sur} with the MacCready (2007) model, which uses the Pritchard balance, versus time and along-channel coordinate x , where $x = 0$ is the estuary mouth. The white area indicates where s_{sur} is negative. (c) As b, except for the simulation with the model presented in Section 2.2.

166

2.2 Model formulation

167

2.2.1 Domain

168

169

170

171

The study area consists of two parts: an estuary and the adjacent sea. We use x as the along-channel coordinate, where $x = -L_e$ is the upstream limit, $x = 0$ is the estuary mouth, and $x = L_s$ is the boundary of the adjacent sea. The width of the estuary is

$$b(x) = b_0 \exp\left(\frac{x + L_e}{L_b}\right), \quad (1)$$

172

173

174

where b_0 is the width at the upstream limit and L_b is the e-folding length scale which controls the width convergence. The estuary and the open sea have different values of L_b ; the depth H is constant throughout the domain.

175

2.2.2 Hydrodynamic module

176

177

178

179

180

181

182

The hydrodynamic equations are identical to those in MC07. The equations are averaged over the cross-channel y -coordinate and over the tides. Wind is ignored and the Boussinesq approximation is used, with an equation of state that expresses a linear relation between variations in salinity and variations in density. The only difference with respect to MC07 concerns the boundary condition at the bottom $z = -H$, which is taken to be a partial slip condition (instead of no-slip), as in Dijkstra and Schuttelaars (2021), and reads

$$A_v \frac{\partial u}{\partial z} = S_f u \quad \text{at} \quad z = -H. \quad (2)$$

183

184

185

Here, $S_f = \frac{2A_v}{H}$ is the friction coefficient, A_v is the vertical eddy-viscosity coefficient (assumed constant, see later), u is the along-channel velocity and z is the vertical coordinate. At the upstream limit a river discharge Q is imposed:

$$b_0 \int_{-H}^0 u \, dz = Q \quad \text{at} \quad x = -L_e. \quad (3)$$

186

187

The along-channel velocity u and salinity s are split in their respective depth-averaged parts (denoted by a bar) and depth-dependent parts (denoted by primes):

$$u = \bar{u} + u', \quad s = \bar{s} + s'. \quad (4)$$

188

The solutions of the equations for along-channel velocity read

$$\bar{u} = \frac{Q}{bH}, \quad u' = \bar{u} \left(\frac{1}{5} - \frac{3}{5} \frac{z^2}{H^2} \right) + \alpha \frac{\partial \bar{s}}{\partial x} \left(\frac{8}{5} - \frac{54}{5} \frac{z^2}{H^2} - 8 \frac{z^3}{H^3} \right), \quad (5)$$

189

190

191

192

193

194

195

196

197

198

199

where $\alpha = \frac{g\beta H^3}{48A_v}$. Here, $g = 9.81 \text{ m s}^{-2}$ is gravitational acceleration and β the isohaline contraction coefficient of water ($= 7.6 \times 10^{-4} \text{ psu}^{-1}$). The vertical eddy-viscosity coefficient is parametrized as $A_v = c_v U_T H$, where U_T is the amplitude of the tidal current and $c_v = 7.28 \times 10^{-5}$ is an empirical constant (Ralston et al., 2008). This formulation is based on the assumption that the relevant velocity scale for turbulent mixing in an estuary is the amplitude of the tidal current and the limiting vertical length scale of the turbulent eddies is the depth of the estuary. The physical interpretation of Eq. 5 is that the depth-averaged current is solely due to the river discharge, and that the vertical velocity shear is caused by the river current and the density-driven flow. Hereafter, we will refer to u' as the exchange flow (Geyer & MacCready, 2014). The vertical velocity w follows from continuity,

$$\frac{\partial}{\partial x} (bu) + \frac{\partial}{\partial z} (bw) = 0, \quad (6)$$

200

which results in

$$w = \alpha H \left(\frac{\partial^2 \bar{s}}{\partial x^2} + L_b^{-1} \frac{\partial \bar{s}}{\partial x} \right) \left(2 \frac{z^4}{H^4} + \frac{18}{5} \frac{z^3}{H^3} - \frac{8}{5} \frac{z}{H} \right). \quad (7)$$

2.2.3 Salt module

The salt conservation equation is

$$\frac{\partial s}{\partial t} + \frac{1}{b} \frac{\partial}{\partial x} (bus) + \frac{\partial}{\partial z} (ws) = \frac{1}{b} \frac{\partial}{\partial x} (bK_h s) + \frac{\partial}{\partial z} (K_v \frac{\partial s}{\partial z}) \quad (8)$$

where t is time. The horizontal eddy-diffusion coefficient is parametrized as $K_h = c_h U_T b$, where $c_h = 0.035$ is an empirically determined constant (Banas et al., 2004). A closure relation for the vertical eddy-diffusion coefficient K_v is $K_v = \frac{A_v}{Sc}$, with $Sc = 2.2$ the Schmidt number (Ralston et al., 2008). At the upstream limit ($x = -L_e$) a river salinity s_{ri} imposed. The simulated domain stretches well beyond the limit of salt intrusion, to avoid that this condition affects the salinity dynamics in the estuary. In the part that represents the adjacent sea, width increases strongly with distance to the mouth, so that the river flow will become very weak at the sea boundary $x = L_s$. This allows us to assume that at this downstream boundary of the domain (located seaward of the estuary mouth at $x = 0$) salinity will be well-mixed over the vertical and we can set salinity to be equal to the ocean salinity s_{oc} over the entire depth. Hence,

$$s|_{x=-L_e} = s_{ri}, \quad s|_{x=L_s} = s_{oc}. \quad (9)$$

At the bottom and the free surface the vertical salt flux vanishes:

$$K_v \frac{\partial s}{\partial z} = 0 \quad \text{at } z = -H \text{ and } z = 0. \quad (10)$$

At the transition between the parts at $x = 0$, both s and the salt transport $b(us - K_h \frac{\partial s}{\partial x})$ have to be continuous. Since u and b are continuous, this last condition implies that $\frac{\partial s}{\partial x}$ has to be continuous as well. This can be written as

$$\lim_{x \uparrow 0} s = \lim_{x \downarrow 0} s, \quad \lim_{x \uparrow 0} \frac{\partial s}{\partial x} = \lim_{x \downarrow 0} \frac{\partial s}{\partial x}. \quad (11)$$

2.2.4 Solution method

To solve for salinity, Eq. 4 is inserted into Eq. 8 and this equation is averaged over the depth, resulting in the depth-averaged salt balance:

$$\underbrace{\frac{\partial \bar{s}}{\partial t}}_{T_1} + \underbrace{\frac{1}{b} \frac{\partial}{\partial x} (b\bar{u}\bar{s})}_{T_2} + \underbrace{\frac{1}{b} \frac{\partial}{\partial x} (b\overline{u's'})}_{T_3} - \underbrace{\frac{1}{b} \frac{\partial}{\partial x} (bK_h \frac{\partial \bar{s}}{\partial x})}_{T_4} = 0. \quad (12)$$

Here T_1 is the tendency term. Terms T_2 - T_4 contain along-channel variations of three width-integrated and depth-mean salt fluxes: that due to river flow (T_2), due to exchange flow (T_3 , which can be split into a contribution by the density-driven current and a contribution induced by the river current) and a diffusive flux (T_4). The equation for the evolution of s' is found by subtracting Eq. 12 from Eq. 8, yielding

$$\underbrace{\frac{\partial s'}{\partial t}}_{T_5} + \underbrace{\bar{u} \frac{\partial s'}{\partial x}}_{T_6} + \underbrace{u' \frac{\partial s'}{\partial x}}_{T_7} + \underbrace{u' \frac{\partial \bar{s}}{\partial x}}_{T_8} - \underbrace{\frac{1}{b} \frac{\partial}{\partial x} (b\overline{u's'})}_{T_9} + \underbrace{w \frac{\partial s'}{\partial z}}_{T_{10}} - \underbrace{\frac{\partial}{\partial z} (K_v \frac{\partial s'}{\partial z})}_{T_{11}} - \underbrace{\frac{1}{b} \frac{\partial}{\partial x} (bK_h \frac{\partial s'}{\partial x})}_{T_{12}} = 0. \quad (13)$$

Term T_5 is the tendency term. Terms T_6 and T_7 represent the horizontal advection of s' and T_8 the creation of stratification by vertical velocity shear. Term T_9 is equal to minus T_3 , T_{10} represents vertical advection, T_{11} vertical diffusion and finally T_{12} represents horizontal diffusion. Note that when the Pritchard balance is applied, only terms T_8 and T_{11} are taken into account in Eq. 13.

This set of equations is solved for \bar{s} and s' . To deal with the vertical variations, a Galerkin method (see e.g. Canuto et al. (2012)) is used. For this, the depth-dependent

233 salinity is written as a Fourier series

$$s' = \sum_{n=1}^N s_n(x, t) \cos\left(\frac{n\pi}{H} z\right), \quad (14)$$

234 where N is the number of vertical modes and s_n are the Fourier components, which de-
 235 pend on the horizontal coordinate x and on time t . This expression is substituted in to
 236 Eq. 13, and afterwards this equation is projected onto the Fourier modes. Combined with
 237 Eq. 12, this yields $N+1$ equations for $\bar{s}(x, t)$ and the $s_n(x, t)$, $n = 1, 2, \dots, N$, which are
 238 numerically solved by using central differences on a spatially uniform grid in x , while time
 239 integration is performed with the Crank-Nicolson method (Crank & Nicolson, 1947). This
 240 results in a system of $N+1$ algebraic equations at every grid point, containing values
 241 of \bar{s} and s_n at the previous and current timestep. This system of equations is solved with
 242 the Newton-Raphson method (see e.g. Galántai (2000)).

243 2.3 Performance of the model

244 The new model is next used to simulate the same freshwater pulse in the Guadalquivir
 245 Estuary, as was done with the MC07 model. Model settings are the same as in Section
 246 2.1. Additionally, the number of vertical modes is chosen as $N = 10$ and the sea do-
 247 main is modeled as a 25 km long channel with an e-folding length scale of 2.5 km. As
 248 the numerical scheme is now implicit, it allows for larger timesteps. A standard value
 249 of $\Delta t = 12$ hours is chosen, but to guarantee accuracy a smaller Δt is chosen when the
 250 salt field changes fast. When the change in salinity is large, the Newton-Raphson algo-
 251 rithm may not converge for too large timesteps. When this happens, also a smaller timestep
 252 is chosen; a minimum timestep of 15 minutes is used.

253 Results from this simulation are displayed in Fig. 1c. Before and after the fresh-
 254 water pulse, salt intrusion is stronger than in the simulation with the MC07 model (Fig. 1b).
 255 However, during the pulse, no negative values of salinity are simulated, which indicates
 256 that our model has overcome the problematic behavior of the MC07 model when sim-
 257 ulating strong freshwater pulses. To check the numerical accuracy of the solutions, ad-
 258 ditional simulations were done where the time and spatial resolution were taken twice
 259 as small and with the number of vertical modes increased to $N = 15$. The maximum
 260 difference in salinity between the simulations was smaller than 0.01 psu, assuring that
 261 the results are sufficiently accurate.

262 There are three possible explanations for the difference between the MC07 model
 263 and the new model: the different boundary condition for momentum at the bottom, the
 264 different boundary condition for salinity at the sea boundary (and the inclusion of the
 265 sea domain) or the generalized equation for the evolution of s' . First, to determine whether
 266 the boundary condition for momentum is the cause, an additional simulation was done
 267 where the no-slip boundary condition from MC07 was used as a boundary condition for
 268 momentum. In this simulation, salt intrusion before and after the pulse is smaller than
 269 in the simulation with the partial slip boundary condition, but no negative salinity val-
 270 ues were simulated. Second, the effect of the boundary condition for salinity at the sea
 271 boundary was investigated by calculating the value of salinity at the bottom at the es-
 272 tuary mouth. This has a minimum value of 32.8 psu, which is a relatively small ($\approx 10\%$)
 273 deviation from the prescribed value in the MC07 model. Third, the effect of the addi-
 274 tional terms in Eq. 13 was studied. Fig. 2 displays the terms in this equation during the
 275 simulation. It is clear that the largest terms during the entire simulation are T_8 and T_{11} ,
 276 which are the only terms taken into account in MC07. However, during the pulse, also
 277 other terms become important, in particular T_{10} , the vertical (upward) advection of salt.
 278 This explains why negative salinity can occur in MC07: the amount of destruction of strat-
 279 ification by vertical mixing during freshwater pulses is too small compared to the crea-
 280 tion by vertical shear. This leads to an overestimation of stratification in MC07, lead-
 281 ing to negative salinity in the surface layer.

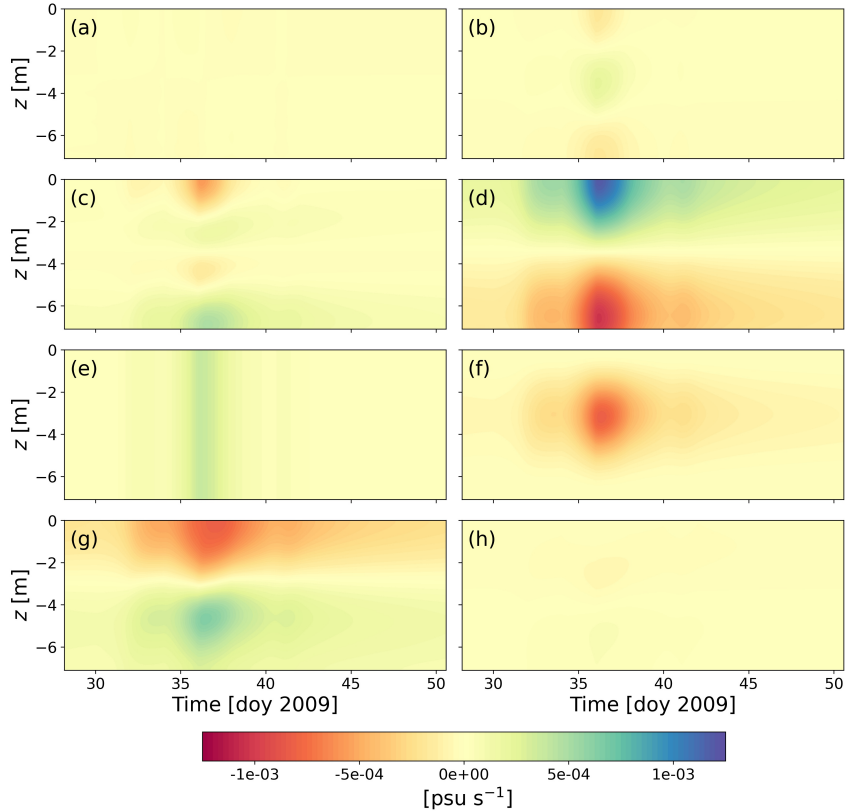


Figure 2. The magnitudes of the different terms in Eq. 13 versus time and depth in the first grid cell upstream of $x = 0$ during the simulation of the February 2009 freshwater pulse in the Guadalquivir Estuary with our model. a) T_5 , b) T_6 , c) T_7 , d) T_8 , e) T_9 , f) T_{10} , g) T_{11} and h) T_{12} .

282

2.4 Set-up of the numerical experiments

283

284

285

286

287

288

289

290

291

292

293

294

295

296

297

298

Next, the model is used to study the sensitivity of the estuarine salinity response to freshwater pulses. For this a model domain is chosen that is a straight channel with a width of 1000 m and a depth of 10 m. The adjacent sea part is 25 km long and it has a convergence length of 2.5 km. This setting is chosen to mimic an ‘average’ coastal plain estuary. Sea salinity is 35 psu and river salinity is 0 psu. The horizontal grid size varies between a minimum of 125 m and maximum of 500 m for different simulations and the number of vertical modes ranges from 5 to 15, depending on the strength of the stratification. The timestep has values between 15 minutes and 24 hours, giving sufficiently accurate solutions. To model a freshwater pulse, an initial state is chosen in which the subtidal estuarine salinity is steady and in equilibrium with the background river discharge Q_{bg} . The pulse starts when the river discharge increases suddenly to its peak value Q_p . The river discharge remains then for a time T_{pulse} at this peak discharge. After the pulse, the river discharge instantly returns to Q_{bg} . Each simulation is continued until the salt intrusion length has recovered to its initial value. The salt intrusion length X_2 is defined as the distance between the estuary mouth and the most upstream position where the salinity exceeds 2 psu.

299

300

301

302

To quantify the salinity response to a freshwater pulse, several output quantities are defined: change in salt intrusion length ΔX_2 , adjustment time T_{adj} and recovery time T_{rec} . Change in salt intrusion length ΔX_2 is the difference between the value of the salt intrusion length before the pulse and its minimum value during the pulse. Adjustment

303 time T_{adj} is defined as $X_2(t = T_{adj}) = X_2(t = 0) - 0.9\Delta X_2$, which is the time it takes
 304 for the salinity in the estuary to adjust to the peak river discharge. Recovery time T_{rec}
 305 is the time after the pulse when $X_2(t = T_{rec}) = X_2(t = 0) - 0.1\Delta X_2$, so it is the time
 306 when 90% of the recovery of X_2 after the pulse has taken place. These quantities are scaled
 307 to make the resulting dependencies more general. As a scale for ΔX_2 , the background
 308 salt intrusion length $X_2(t = 0)$ is used. For T_{adj} , the adjustment time found by Kranenburg
 309 (1986) is used as a scale, which reads $T_{adj,sc} = \frac{0.9bH\Delta X_2}{Q_p}$. The factor 0.9 accounts for
 310 the fact that here T_{adj} is defined when 90% of the change in X_2 has occurred. Finally,
 311 the scale for T_{rec} is $T_{rec,sc} = \frac{0.9bHX_2(t=0)}{Q_{bg}}$. This is the timescale that results from the
 312 assumption that recovery is primarily due to salt transport by the exchange flow. Clas-
 313 sical theory (Chatwin, 1976) is applied, i.e., $\overline{u's'}$ during the recovery is approximately
 314 balanced by salt transport due to river flow. The factor 0.9 is added for the same reason
 315 as that in the formulation of $T_{adj,sc}$.

316 The research questions as formulated in the introduction separated the quantifi-
 317 cation of the estuarine salinity response to freshwater pulses into three parts: the sensi-
 318 tivity to the background state (research question 1), the sensitivity to the peak river
 319 discharge (research question 2) and the sensitivity to the duration of the pulse (research
 320 question 3). These different research questions motivate the variation of four dimensional
 321 parameters: U_T, Q_{bg}, Q_p and T_{pulse} . These are converted into four dimensionless param-
 322 eters, which are $Fr_T, Fr_{R,bg}, Fr_{R,p}$ and \tilde{T}_{pulse} . Here, $Fr_T = \frac{U_T}{c}$ is the tidal Froude num-
 323 ber, with $c = \sqrt{g\beta H s_{oc}}$ an internal velocity scale that equals twice the maximum in-
 324 ternal wave speed. Furthermore, $Fr_{R,bg} = \frac{Q_{bg}}{bHc}$ is defined as the background freshwa-
 325 ter Froude number and $Fr_{R,p} = \frac{Q_p}{bHc}$ the peak freshwater Froude number. Finally, $\tilde{T}_{pulse} =$
 326 $\frac{T_{pulse}}{T_{adj}}$ is the scaled duration of the pulse.

327 Specifically, for addressing research question 1, a number of simulations is performed
 328 where $Fr_{R,p}$ is fixed and Fr_T and $Fr_{R,bg}$ are varied, since these two quantities are shown
 329 to determine the equilibrium state of an estuary (Geyer & MacCready, 2014). The dura-
 330 tion of the pulse is chosen to exceed the adjustment time, so equilibrium with the peak
 331 river discharge is reached during the pulse. This set of simulations will be referred to as
 332 experiment set *Background*. For answering research question 2, $Fr_{R,bg}$ and $Fr_{R,p}$ are
 333 varied. The tidal Froude number Fr_T is fixed at a value of 0.62 ($U_T = 1 \text{ m s}^{-1}$). The
 334 duration of the pulse T_{pulse} again exceeds the adjustment time. This set of simulations
 335 will be referred to as experiment set *Peak*. For addressing research question 3, the dura-
 336 tion of the pulse is varied, as well as $Fr_{R,bg}$ and $Fr_{R,p}$. The tidal Froude number Fr_T
 337 is again fixed at 0.62. The values of $Fr_{R,bg}$ and $Fr_{R,p}$ are equal to those in set *Peak*. Two
 338 series of simulations are done where $\tilde{T}_{pulse} = \frac{1}{2}$ and $\frac{1}{4}$. These simulations will be re-
 339 ferred to as experiment set *Short*. Table 1 contains the range of values of the dimensional
 340 parameters for all the experiments that were conducted.

341 The range of the parameters is based on the following. The amplitude of the tidal
 342 current U_T is chosen between 0.75 and 1.5 m s^{-1} , which results in Fr_T ranging from 0.46
 343 to 0.93. Weaker tides are not investigated, because the momentum balance relies on the
 344 assumption of moderate to strong tidal currents with respect to the river current. Larger
 345 tidal currents are not investigated because they are considered to be non-realistic. The
 346 range of values of the freshwater Froude numbers is based on daily discharge values from
 347 five estuaries where freshwater pulses are identified. The considered estuaries are the Gironde
 348 (France), the Guadiana (Spain/Portugal), the Guadalquivir (Spain), San Francisco Bay
 349 (USA) and the Tagus (Portugal). Specifics of the river discharge datasets are given in
 350 Table 2. Freshwater pulses are identified in the river discharge datasets and displayed
 351 in $(Fr_{R,p}, Fr_{R,bg})$ parameter space in Fig. 3. Based on these observations, a value of $Fr_{R,p} =$
 352 0.15 is chosen as a standard value for the simulations of experiment set *Background*. Since
 353 a freshwater pulse is defined here as an event when the river discharge exceeds three times
 354 its long-yearly average value, an obvious upper bound for $Fr_{R,bg}$ is 0.05 for this set of
 355 experiments, one-third of the value of $Fr_{R,p}$. The lower bound is $Fr_{R,bg} = 0.001$. For

356 experiment set *Peak*, values of $Fr_{R,bg}$ range from 0.001 to 0.075 and those of $Fr_{R,p}$ range
 357 between 0.02 and 0.3. These boundaries are indicated by the black lines in Fig. 3. The
 358 majority of the observed freshwater pulses fit within these boundaries, but not all of them.
 359 Observed pulses for which $3 Fr_{R,bg} > Fr_{R,p}$ probably started far from a steady state
 360 (shortly before the pulse, another pulse occurred) and are thus not considered. The strongest
 361 freshwater pulses in the Guadalquivir and Guadiana have $Fr_{R,p} > 0.3$ and are also out-
 362 side the investigated parameter space. This is done because multiple model assumptions
 363 are not valid anymore under such extreme circumstances, in particular the width and
 364 depth being constant. Such strong freshwater pulses will increase the water level signif-
 365 icantly and flood lands next to the estuary. Moreover, simplifying assumptions regard-
 366 ing the momentum balance, which rely on the estuary being partially to well mixed, do
 367 not hold during such extreme events.

Table 1. Amplitude of tidal current U_T , background river discharge Q_{bg} , peak river discharge Q_p and duration of the pulse T_{pulse} for the different sets of experiments.

| Parameter | <i>Background</i> | <i>Peak</i> | <i>Short</i> |
|--|-------------------|-------------|---|
| U_T [m s ⁻¹] | 0.75-1.5 | 1.0 | 1.0 |
| Q_{bg} [m ³ s ⁻¹] | 16-808 | 16-1211 | 16-1211 |
| Q_p [m ³ s ⁻¹] | 2423 | 323-4846 | 323-4846 |
| T_{pulse} | $> T_{adj}$ | $> T_{adj}$ | $\frac{1}{4}T_{adj}$, $\frac{1}{2}T_{adj}$ |

Table 2. Specifications of river discharge datasets for five estuaries where freshwater pulses occur. For the Gironde, river discharge from the Garonne and Dordogne are added. For the San Francisco Bay, the dataset combines multiple sources.

| Estuary | Station | Produced by | Period |
|-------------------|------------------------------------|---|-----------|
| Gironde | Lamonzie-Saint-Martin and Tonneins | Banque Hydro | 2001-2020 |
| Guadiana | Pulo do Lobo | Portuguese Water Institute | 1947-2020 |
| Guadalquivir | Alcalá del Rio dam | Agencia de Medio Ambiente y Agua de Andalucía | 1931-2011 |
| San Francisco Bay | Net outflow | California Department of Water Resources | 1929-2020 |
| Tagus | Ómnias (Santarém) | Portuguese Water Institute | 1972-2002 |

368 3 Results and discussion

369 3.1 Sensitivity analysis

370 Results of experiment set *Background* are displayed in Fig. 4. Panels show the de-
 371 pendence of background salt intrusion length, change in salt intrusion length, adjustment
 372 time and recovery time on the tidal Froude number Fr_T and background freshwater Froude
 373 number $Fr_{R,bg}$. Note that intensity and duration of the freshwater pulse are kept fixed
 374 (Table 1). Clearly, all dimensional response characteristics (contours in Fig. 4) become
 375 lower for higher Fr_T and higher $Fr_{R,bg}$. The scaled quantities in panels 4b-d show a dif-
 376 ferent behavior: they only weakly depend on Fr_T and for increasing $Fr_{R,bg}$ the relative

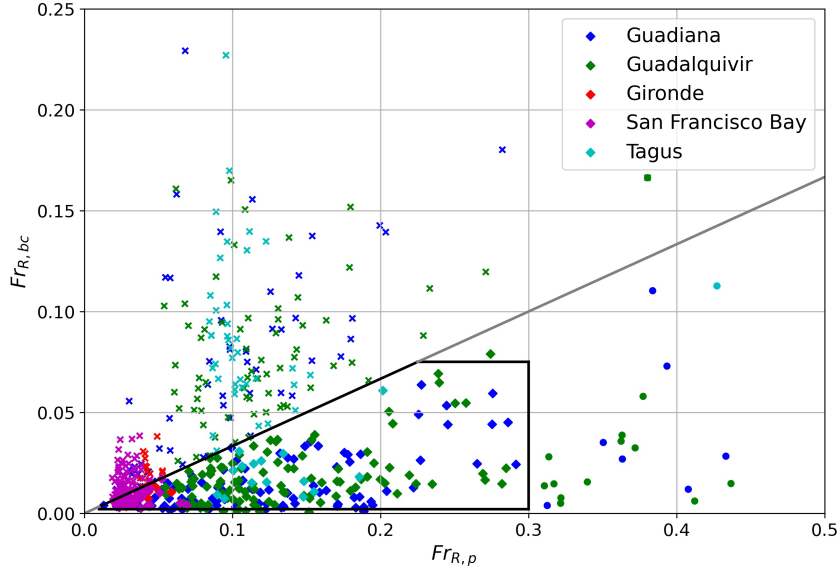


Figure 3. Observed freshwater pulses in the $Fr_{R,p}, Fr_{R,bg}$ parameter space. The cross-shaped markers are freshwater pulses where the peak river discharge is less than three times the background river discharge, the diamond-shaped markers indicate events where the peak river discharge exceeds this value and the circular markers indicate freshwater pulses where $Fr_{R,p} > 0.3$. The grey line is where $Fr_{R,p} = 3 Fr_{R,bg}$. The black box indicates the part of the parameter space that was investigated by experiments *Peak* and *Short*.

377
378

change in salt intrusion length decreases, whilst the scaled adjustment and recovery time increase.

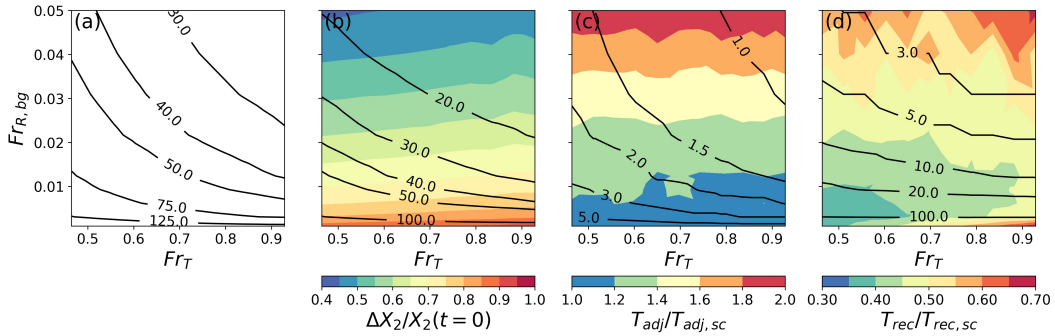


Figure 4. Results of experiment set *Background*. (a) Contour plot of background salt intrusion length $X_2(t = 0)$ (values in km) as a function of tidal Froude number Fr_T and background freshwater Froude number $Fr_{R,bg}$. (b) As panel a, except for the change in salt intrusion length ΔX_2 (contours, values in km) and the change in the scaled salt intrusion length $\Delta X_2/X_2(t = 0)$ (colors). (c). As panel b, except for the adjustment time T_{adj} (contours, values in days) and the scaled adjustment time $T_{adj}/T_{adj,sc}$ (colors). (d) As panel c, except for the recovery time T_{rec} and the scaled recovery time $T_{rec}/T_{rec,sc}$.

379 The dependence of background salt intrusion length $X_2(t=0)$ on Fr_T and $Fr_{R,bg}$
 380 (Fig. 4a) follows the power-law relationship $X_2(t=0) \sim Fr_{R,bg}^{-1/3} Fr_T^{-1}$, according
 381 to classical theory on estuarine salt dynamics, in which a dominant balance is assumed
 382 between salt export by river flow and salt import by exchange flow (Hansen & Rattray,
 383 1965; Chatwin, 1976; Geyer & MacCready, 2014). However, for low values of the river
 384 flow ($Fr_{R,bg} < 0.005$), horizontal diffusion of salt is important, next to the salt import
 385 by exchange flow, and this power-law is not valid. Excluding this regime, a least squares
 386 fit to the numerical results yields $X_2(t=0) \sim Fr_{R,bg}^{-0.40 \pm 0.03} Fr_T^{-1.00 \pm 0.16}$, in good
 387 agreement with classical theory. This theory also explains the patterns found in Fig. 4b,
 388 as it predicts that $\Delta X_2 \sim (Fr_{R,p}^{-1/3} - Fr_{R,bg}^{-1/3}) Fr_T^{-1}$, while a least squares fit to the data
 389 yields $\Delta X_2 \sim (Fr_{R,p}^{-0.28 \pm 0.00} - Fr_{R,bg}^{-0.31 \pm 0.01}) Fr_T^{-0.89 \pm 0.01}$. Also, it follows that $\Delta X_2/X_2(t=$
 390 $0)$ is independent of Fr_T .

391 The patterns shown in Fig. 4c,d can be understood by identifying and analyzing
 392 the processes that act during adjustment and recovery. Fig. 4c shows that for $Fr_{R,bg} <$
 393 0.015 the adjustment time $T_{adj} \simeq T_{adj,sc}$. In this ‘high-pulse regime’, where the peak
 394 river discharge is relatively large compared to the background river discharge, the dom-
 395 inant process for adjustment is the export of salt by river flow during the pulse. In the
 396 ‘moderate-to-low pulse regime’ (the upper part of the panel) T_{adj} is considerably larger
 397 than $T_{adj,sc}$. During the adjustment, other salt transport mechanisms are then effective
 398 as well, viz. import of salt by both the exchange flow and by horizontal diffusion. As they
 399 oppose the salt export by river flow, the adjustment time is larger than that would re-
 400 sult from river flow alone. The fact that the value of Fr_T does affect the dimensional
 401 adjustment time but not the scaled adjustment time indicates that its effect is mostly
 402 through a larger change in salt intrusion length (see panel b), but that the celerity of the
 403 adjustment is not sensitive to Fr_T .

404 A similar reasoning applies to the recovery time: it will be close to the scaled value
 405 $T_{rec,sc}$ if the recovery process is controlled by salt transport due to the exchange flow,
 406 as described by the classical theory. Fig. 4d shows that this only approximately holds
 407 in the ‘weak pulse regime’, i.e., in the upper part of the diagram. For moderate to stronger
 408 pulses, values of the recovery time are approximately half of $T_{rec,sc}$. This deviation from
 409 quasi-steady classical theory exists because immediately after the pulse, the landward
 410 salt transport due to exchange flow is substantially larger than the seaward transport
 411 by river flow. A larger value of Fr_T , i.e. stronger tidal mixing, will result in slower re-
 412 covery, because the magnitude of the exchange flow is inversely proportional to the value
 413 of U_T . Yet the recovery time is not very sensitive to the value of U_T because this effect
 414 is compensated by the fact that the change in salt intrusion length also decreases approx-
 415 imately linearly for higher U_T .

416 To look at this in more detail, we present results of the change in salt content of
 417 an estuary for different values of the background river discharge and of the tidal current
 418 amplitude. The integrated salt balance is obtained by integrating Eq. 12 over the vol-
 419 ume of the estuary:

$$\underbrace{\frac{d}{dt} \int_{-L_e}^0 \rho_0 b H \bar{s} \, dx}_{S_1} = \rho_0 b H \left(\underbrace{\bar{u} \bar{s}}_{S_2} + \underbrace{\bar{u}' s'}_{S_3} - \underbrace{K_h \frac{\partial \bar{s}}{\partial x}}_{S_4} \right) \Big|_{x=0}. \quad (15)$$

420 Here, it is assumed that salt transport vanishes at the upstream limit. Term S_1 repre-
 421 sents time rate of change of salt content in the estuary, and S_2 - S_4 are depth-averaged
 422 salt fluxes at the estuary mouth due to river flow, exchange flow and horizontal diffu-
 423 sion, respectively. Fig. 5 shows time series of the river discharge, salt intrusion lengths
 424 and terms S_2 , S_3 and S_4 .

425 Fig. 5a reveals that the adjustment of the salt intrusion length to a freshwater pulse
 426 is to a good approximation linear in time. Panel b shows that the magnitude of the salt

427 flux due to exchange flow (S_3) is indeed larger during the adjustment for higher values
 428 of Q_{bg} , which slows down the adjustment. The diffusive salt flux S_4 is small compared
 429 to the other fluxes for all cases. Panel c and d reveal that higher values of U_T cause a
 430 smaller change in salt intrusion length, but that the magnitudes of the salt fluxes into
 431 the estuary during the adjustment are only slightly affected by the different value of U_T ,
 432 which is in line with the results shown in Fig. 4c.

433 Regarding the recovery time, we see that a substantial part of the recovery takes
 434 place in the first few days after the pulse (Fig. 5a). This means that just after the pulse
 435 the salt transport due to exchange flow is very important for the total recovery time. The
 436 value of $T_{rec,sc}$ is calculated by assuming this transport scales with the transport of salt
 437 by the background river flow, which is not a good estimate during this period, especially
 438 for strong pulses. Thus T_{rec} will be shorter than $T_{rec,sc}$ for strong pulses, which is in-
 439 deed found. The effect of U_T is clearly illustrated in Fig. 5c and d: a lower value of U_T
 440 means that the change in salt intrusion length is larger (panel c), but also the salt flux
 441 due to exchange flow S_3 is stronger (panel d) and these effects compensate each other.

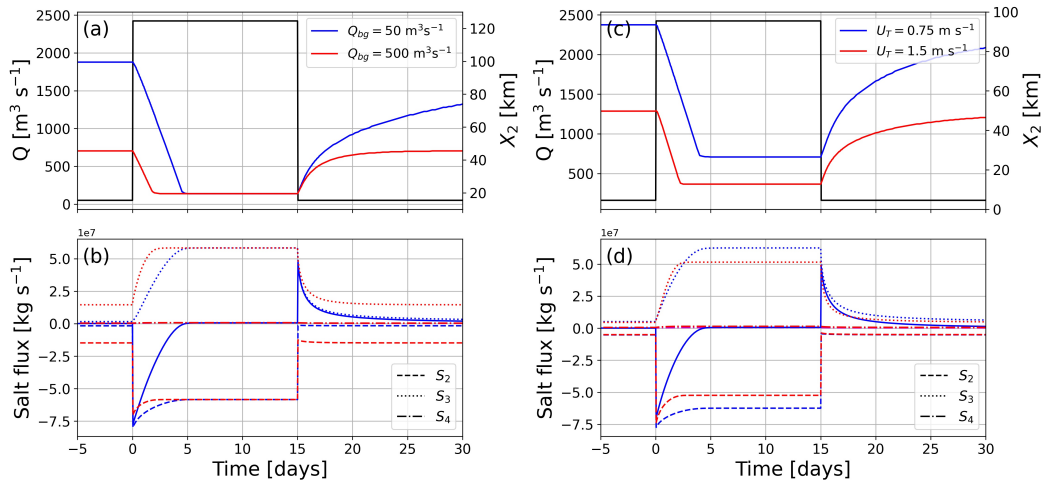


Figure 5. (a) Time series of river discharge (black line) and salt intrusion length (coloured lines) for different background river discharges Q_{bg} . Only the discharge for the case $Q_{bg} = 50 m^3 s^{-1}$ is plotted. These simulations are from experiment set *Background* (i.e. $Q_p = 2423 m^3 s^{-1}$). (b) Time series of the different terms at the right-hand side of Eq. 15. The colours refer to the same simulations as in panel (a). (c)-(d) As (a)-(b), except for different values of U_T .

442 Results of experiment set *Peak* are shown in Fig. 6. The same quantities as in Fig. 4
 443 are displayed, except now for different values of $Fr_{R,bg}$ and $Fr_{R,p}$, while the amplitude
 444 of the tidal current and duration of the freshwater pulse are kept fixed (Table 1). Panel
 445 a shows background salt intrusion lengths for reference purposes. Panels b and c show
 446 the same patterns as in experiment set *Background*: with increasing strength of the pulses
 447 the change in salt intrusion length becomes larger and the adjustment time becomes smaller.
 448 The recovery time barely depends on the value of $Fr_{R,p}$ (panel d).

449 The patterns in parameter space in experiment set *Background* are mostly explained
 450 by whether a pulse is ‘weak’ or ‘strong’, i.e. from the ratio between $Fr_{R,bg}$ and $Fr_{R,p}$.
 451 Regarding the change in salt intrusion length, its dependence on $Fr_{R,p}$ follows again from
 452 the fact that $\Delta X_2/X_2(t=0) \sim 1 - (\frac{Fr_{R,bg}}{Fr_{R,p}})^{\frac{1}{3}}$. This behaviour is visible in Fig. 6b.
 453 A least-squares fit to this data yields an exponent of 0.43 ± 0.01 in this relation, dis-
 454 playing the validity of classical theory.

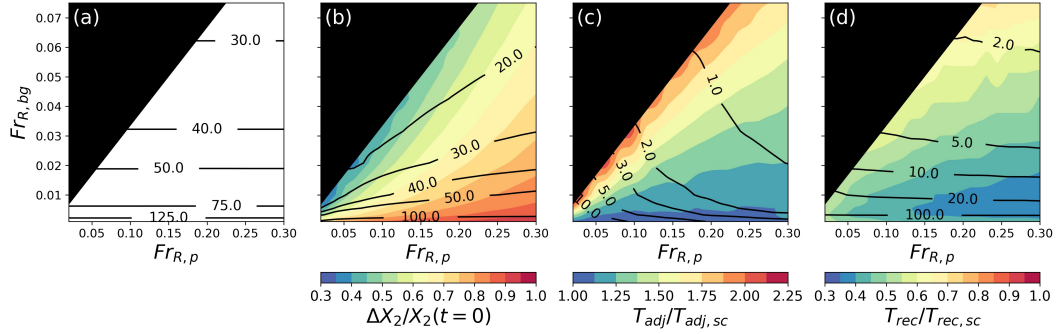


Figure 6. Results of experiment set *Peak*. (a) Contour plot of background salt intrusion length $X_2(t = 0)$ (values in km) as a function of peak freshwater Froude number $Fr_{R,p}$ and background freshwater Froude number $Fr_{R,bg}$. (b) As panel a, except for the change in salt intrusion length ΔX_2 (contours, values in km) and the scaled change in salt intrusion length $\Delta X_2/X_2(t = 0)$ (colors). (c). As panel b, except for the adjustment time T_{adj} (contours, values in days) and the scaled adjustment time $T_{adj}/T_{adj,sc}$ (colors). (d) As panel c, except for the recovery time T_{rec} and the scaled recovery time $T_{rec}/T_{rec,sc}$. The black area indicates where $Fr_{R,p} < 3 Fr_{R,bg}$.

455 The adjustment time follows the Kranenburg (1986) theory for strong pulses, as
 456 is seen by values of the scaled adjustment time ($T_{rec}/T_{rec,sc}$) $\simeq 1$ in the lower right part
 457 of Fig. 6c. For weaker pulses the import of salt due to the exchange flow during the ad-
 458 justment can not be ignored and the adjustment is slower, leading to higher values of
 459 the scaled adjustment time when going to the left or upwards in this figure.

460 The strong dependence of the exchange flow on the salinity gradient explains why
 461 the recovery time hardly depends on the peak river discharge. Since the salinity gradi-
 462 ent is larger after a pulse with a high value of Q_p , the recovery due to the exchange flow
 463 will be faster. This is compensated by the larger change in salt intrusion length for a larger
 464 Q_p .

465 To illustrate the previous statements regarding time scales, Fig. 7 displays salt in-
 466 trusion lengths (panel a) and S_2 , S_3 and S_4 of Eq. 15 (panel b) for different values of peak
 467 river discharge. Regarding the adjustment time, Fig. 7b shows that during adjustment
 468 to the peak river discharge the salt flux due to exchange flow (S_3) is relatively stronger
 469 for weaker pulses. The rate of recovery immediately after the pulse is higher for the larger
 470 pulse, leading to a similar situation for both cases after a few days and thus pulses with
 471 different strengths have approximately the same recovery time.

472 Finally, results for experiment set *Short* are displayed in Fig. 8. Panels a and b show
 473 the values of change in salt intrusion length for different values of $Fr_{R,p}$ and $Fr_{R,bg}$ and
 474 for two durations of the pulse, with Fr_T fixed. It appears that the change in salt in-
 475 trusion length depends approximately linearly on the duration of the pulse. This is the case
 476 for all values of $Fr_{R,p}$ and $Fr_{R,bg}$. Panels c and d show that the recovery time T_{rec} barely
 477 depends on the duration of the pulse.

478 The linear dependence of ΔX_2 on T_{pulse} is a consequence of the fact that the time
 479 rate of change of X_2 is linear in time during most of the adjustment (Figs. 5 and 7). Thus
 480 the change in salt intrusion length can be estimated from multiplying the downstream
 481 velocity of the salt intrusion with the duration of the pulse. Because of this, ΔX_2 will
 482 indeed depend linearly on T_{pulse} when no equilibrium is reached.

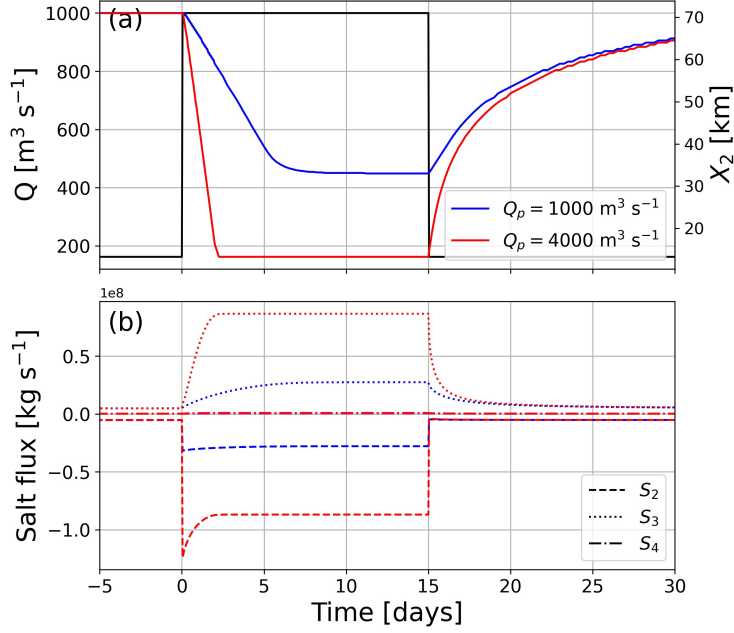


Figure 7. As Fig. 5a-b, except for different values of peak river discharge Q_p from experiment set *Peak*. In panel a only the discharge for the case $Q_p = 1000 \text{ m}^3 \text{ s}^{-1}$ is plotted.

483 The finding that T_{rec} does not depend on T_{pulse} is due to the fact that the exchange
 484 flow is not fully developed before equilibrium with the peak discharge is reached (see Figs. 5
 485 and 7). When the pulse ends at this stage, salt import will thus be weaker compared to
 486 when the pulse would have reached equilibrium. So during the recovery after a shorter
 487 pulse, the upstream velocity of the salt intrusion will be smaller. At the same time, ΔX_2
 488 is also smaller for shorter pulses. These two effects have similar magnitude and will com-
 489 pensate each other.

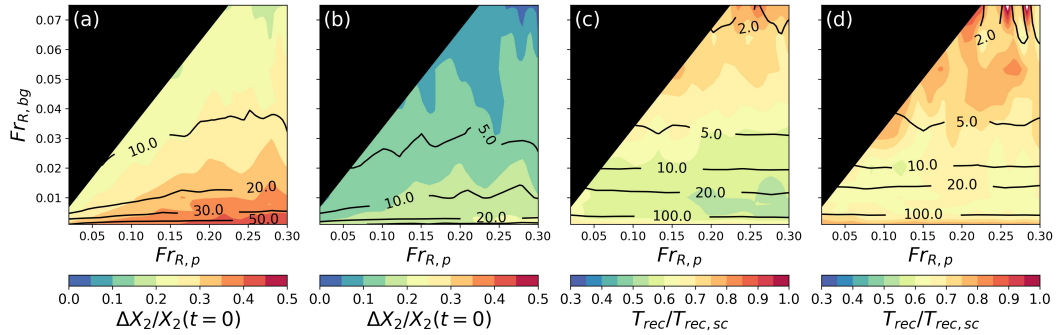


Figure 8. Results of experiment *Short*. (a) Contour plot of change in salt intrusion length ΔX_2 (contours, values in km) and scaled change in salt intrusion length $\Delta X_2/X_2(t=0)$ (colors) a function of peak freshwater Froude number $Fr_{R,p}$ and background freshwater Froude number $Fr_{R,bg}$ for $T_{pulse} = \frac{1}{2}T_{adj}$. (b) As panel a, except for $T_{pulse} = \frac{1}{4}T_{adj}$. (c) As panel a, except for the recovery time T_{rec} (contours, values in days) and the scaled recovery time $T_{rec}/T_{rec,sc}$ (colours). (d) As panel c, except for $T_{pulse} = \frac{1}{4}T_{adj}$. The black area indicates where $Fr_{R,p} < 3 Fr_{R,bg}$.

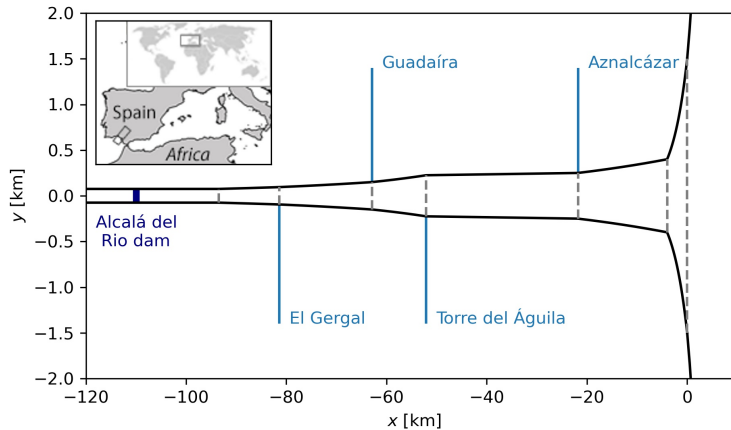


Figure 9. The geometry of the Guadalquivir Estuary used for the simulation. The most upstream and downstream domains are not entirely plotted, because of their extent in the x - and y -direction, respectively.

490

3.2 Specific application

491

492

493

494

495

496

497

498

499

In this section the model performance is assessed by applying it to observed freshwater pulses in the Guadalquivir Estuary. For this purpose, the model was slightly extended to a new geometry that consists of multiple (instead of one) estuarine parts, as is shown in Fig. 9. In each of these parts the equations as presented in Section 2.2 are solved. For salinity the matching conditions shown in Eq. 11 are used at the boundaries of the parts. Furthermore, additional river discharge of four tributaries are added at the beginning of each part. The other model settings are equal to those used in Section 2.3, with one exception: for salinity at the river boundary a value of 0.5 psu was used, based on observations.

500

501

502

503

504

505

506

Details about the observations are given in Navarro et al. (2011, 2012). To determine the subtidal salt intrusion length, first a Gaussian filter with a half-amplitude of 12 hours is applied to the raw salinity measurements to average over the tides. Afterwards, the observed salinity (observations are done at the surface) is linearly interpolated between the measurement points and the most upstream point where the salinity exceeds 2 psu is identified. During the observational period, several freshwater pulses occurred: one in February 2009 and a series of three pulses in 2010.

507

508

509

510

511

512

513

514

515

516

517

518

519

520

Simulations are done in order to capture the effects of these pulses. Fig. 10 displays the results of these simulations and the observations in the Guadalquivir. To quantify the differences, the root-mean-square error of the observed and simulated salt intrusion length is calculated, which will be noted as $RMSE(X_2)$. For the 2009 case, $RMSE(X_2) = 9.6$ km. However, this number does not reflect the temporal differences: before day 50 of the year 2009, $RMSE(X_2) = 3.7$ km and after this date it is 15.7 km. For the simulations of the pulses in 2010, we have $RMSE(X_2) = 5.4$ km. These values indicate that the model is capable of simulating the temporal behavior of the salt intrusion length in the Guadalquivir Estuary during freshwater pulses. Clearly, there are differences between simulated and observed salt intrusion length, which could be reduced by applying detailed model tuning. For example, Wang et al. (2014) and Losada et al. (2017) argued that the 2009 freshwater pulse in the Guadalquivir created a mud layer on the bottom of the estuary, which decreased the hydraulic drag. This effect could be taken into account by adjusting the value of the partial slip parameter after the pulse.

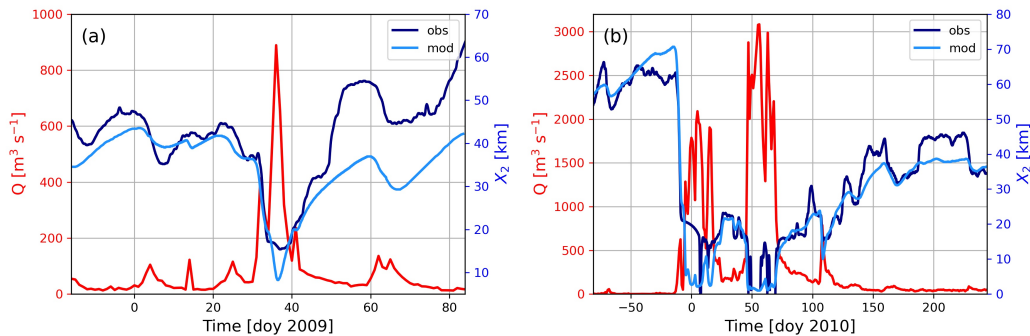


Figure 10. Time series of observed river discharge Q and observed and simulated salt intrusion length X_2 for the Guadalquivir Estuary. The discharge (the red line) is the sum of the main river plus the four tributaries. The dark blue line is the observed X_2 and the light blue line is the simulated X_2 . (a) For the freshwater pulse in 2009. (b) For the series of freshwater pulses in 2010.

521

3.3 Other remarks

522

523

524

525

526

527

528

529

530

531

532

533

534

535

An interesting difference between the results presented here and existing literature concerns the recovery time. Here, we find that this quantity depends only on the river discharge during the recovery, whereas in previous studies (e.g. Kranenburg (1986); Hetland and Geyer (2004); Chen (2015); Monismith (2017)) it is stated that it depends on the change in salt intrusion length. The reason for this difference is that Kranenburg (1986) assumes that during the recovery the exchange flow does not vary in time. However, here we show that the evolution in time of the exchange flow during the recovery is important for the recovery time (Fig. 5 and Fig. 7). Chen (2015) accounts of time-varying exchange flow, but he estimates recovery time from linearized equations, thereby assuming small changes in exchange flow. Our study, on the other hand, clearly shows that these changes are large. Finally, Monismith (2017) accounts for large changes in exchange flow during recovery, but he assumes that depth-averaged salinity at the estuary mouth equals ocean salinity. Certainly, during strong freshwater pulses that condition is too restrictive.

536

537

538

539

540

541

542

543

544

545

Finally, we remark that the estuarine salt response to pulses with a duration that is shorter than the adjustment timescale of the system is not considered in the existing literature. We find that the change in salt intrusion length is linearly related to the duration of the pulse (Fig.8). This is relevant in real estuaries. The duration of freshwater pulses in the observational datasets can be compared to the theoretical adjustment time given by our model. In the smaller estuaries analysed, less than half of the pulses do not reach the equilibrium state (Gadiana: 0.49; Guadalquivir: 0.39; Tagus: 0.38) but in the larger estuaries this portion is even larger (Gironde: 0.76 ; San Francisco Bay: 0.60). So the duration of the pulse is often the limiting factor for the change in salt intrusion length.

546

4 Conclusions

547

548

549

550

551

The aim of this study was to quantify the dependence of the estuarine salinity response to freshwater pulses to the background conditions, the intensity and the duration of the pulse. Application of the MacCready (2007) model, which relies on the Pritchard balance, to observed freshwater pulses in the Guadalquivir Estuary showed that use of this balance results in negative salinity values. We therefore developed a new model, which

552 uses a more detailed description of the vertical salinity structure. Simulations with this
 553 model did not show negative salinity and moreover, the model performs well when ap-
 554 plied to observed freshwater pulses.

555 Model simulations revealed that the influence of the background conditions on the
 556 salinity response to a given freshwater pulse is mainly through the background river dis-
 557 charge; the strength of the tides is of minor importance. Changes in salt intrusion length
 558 ΔX_2 can be estimated successfully from classical theory, but this theory is incorrect re-
 559 garding adjustment time T_{adj} for weak pulses and recovery time T_{rec} for strong pulses.
 560 Simulations with different strengths of the peak river discharge revealed that for ΔX_2
 561 the ratio of peak to background river discharge determines the response. Interestingly,
 562 the peak river discharge is the most important control for T_{adj} while for T_{rec} its value
 563 is not important. When the duration of the freshwater pulse is too small to reach equi-
 564 librium, ΔX_2 will be linearly related to the duration of the pulse, but T_{rec} is not affected.
 565 Observed freshwater pulse characteristics indicate that this control on ΔX_2 is important
 566 in real estuaries.

567 Open Research

568 Software used to generate the data and create the figures used in this study can
 569 be found at git.science.uu.nl/w.y.biemond/code-and-data-freshwater-pulses
 570 [.git](https://git.science.uu.nl/w.y.biemond/code-and-data-freshwater-pulses), as well as the river discharge datasets used. Observational data of the Guadalquivir
 571 Estuary can be found at zenodo.org/record/3459610.

572 Acknowledgments

573 This work is part of the Perspectief Program SaltiSolutions, which is financed by NWO
 574 Domain Applied and Engineering Sciences in collaboration with private and public part-
 575 ners.

576 References

- 577 Banas, N. S., Hickey, B. M., MacCready, P., & Newton, J. A. (2004). Dynamics of
 578 Willapa Bay, Washington: A highly unsteady, partially mixed estuary. *Journal*
 579 *of Physical Oceanography*, *34*(11), 2413 - 2427. doi: 10.1175/JPO2637.1
- 580 Canuto, C., Hussaini, M. Y., Quarteroni, A., Thomas Jr, A., et al. (2012). *Spectral*
 581 *methods in fluid dynamics*. Springer Science & Business Media. doi: 10.1137/
 582 1030157
- 583 Chatwin, P. (1976). Some remarks on the maintenance of the salinity distribution in
 584 estuaries. *Estuarine and Coastal Marine Science*, *4*(5), 555–566. doi: 10.1016/
 585 0302-3524(76)90030-X
- 586 Chen, S.-N. (2015). Asymmetric estuarine responses to changes in river forcing: A
 587 consequence of nonlinear salt flux. *Journal of Physical Oceanography*, *45*(11),
 588 2836–2847. doi: 10.1175/JPO-D-15-0085.1
- 589 Crank, J., & Nicolson, P. (1947). A practical method for numerical evaluation
 590 of solutions of partial differential equations of the heat-conduction type. In
 591 *Mathematical Proceedings of the Cambridge Philosophical Society* (Vol. 43, pp.
 592 50–67). doi: 10.1017/S0305004100023197
- 593 Díez-Minguito, M., Contreras, E., Polo, M., & Losada, M. (2013). Spatio-temporal
 594 distribution, along-channel transport, and post-riverflood recovery of salinity
 595 in the Guadalquivir Estuary (SW Spain) . *Journal of Geophysical Research:*
 596 *Oceans*, *118*(5), 2267–2278. doi: 10.1002/JGRC.20172
- 597 Dijkstra, Y. M., & Schuttelaars, H. M. (2021). A unifying approach to subtidal salt
 598 intrusion modeling in tidal estuaries. *Journal of Physical Oceanography*, *51*(1),
 599 147–167. doi: 10.1175/JPO-D-20-0006.1

- 600 Du, J., & Park, K. (2019). Estuarine salinity recovery from an extreme precipitation
601 event: Hurricane Harvey in Galveston Bay. *Science of the Total Environment*,
602 *670*, 1049–1059. doi: 10.1016/J.SCITOTENV.2019.03.265
- 603 Du, J., Park, K., Dellapenna, T. M., & Clay, J. M. (2019). Dramatic hydrody-
604 namic and sedimentary responses in Galveston Bay and adjacent inner shelf
605 to Hurricane Harvey. *Science of the Total Environment*, *653*, 554–564. doi:
606 10.1016/j.scitotenv.2018.10.403
- 607 Galántai, A. (2000). The theory of Newton’s method. *Journal of Computational and*
608 *Applied Mathematics*, *124*(1-2), 25–44. doi: 10.1016/S0377-0427(00)00435-0
- 609 Geyer, W. R., & MacCready, P. (2014). The estuarine circulation. *Annual Review of*
610 *Fluid Mechanics*, *46*, 175–197. doi: 10.1146/annurev-fluid-010313-141302
- 611 Gong, W., Shen, J., & Reay, W. G. (2007). The hydrodynamic response of the York
612 River estuary to Tropical Cyclone Isabel, 2003. *Estuarine, Coastal and Shelf*
613 *Science*, *73*(3), 695–710. doi: 10.1016/j.ecss.2007.03.012
- 614 Guerra-Chanis, G. E., So, S., & Valle-Levinson, A. (2021). Effects of Hurricane Irma
615 on residual flows and saltwater intrusion in a subtropical estuary. *Regional*
616 *Studies in Marine Science*, *41*, 101568. doi: 10.1016/j.rsma.2020.101568
- 617 Guha, A., & Lawrence, G. A. (2013). Estuary classification revisited. *Journal of*
618 *Physical Oceanography*, *43*(8), 1566–1571. doi: 10.1175/JPO-D-12-0129.1
- 619 Hansen, D. V., & Rattray, M. (1965). Gravitational circulation in straits
620 and estuaries. *Journal of Marine Research*, *23*, 104–122. doi: 10.1357/
621 002224021834614399
- 622 Hetland, R. D., & Geyer, W. R. (2004). An idealized study of the structure of
623 long, partially mixed estuaries. *Journal of Physical Oceanography*, *34*(12),
624 2677–2691. doi: 10.1175/JPO2646.1
- 625 Ingram, R., d’Anglejan, B., Lepage, S., & Messier, D. (1986). Changes in current
626 regime and turbidity in response to a freshwater pulse in the Eastmain estuary.
627 *Estuaries*, *9*(4), 320–325. doi: 10.2307/1351411
- 628 Kranenburg, C. (1986). A time scale for long-term salt intrusion in well-mixed estu-
629 aries. *Journal of Physical Oceanography*, *16*(7), 1329–1331. doi: 10.1175/1520
630 -0485(1986)016(1329:ATSFLT)2.0.CO;2
- 631 Lepage, S., & Ingram, R. G. (1988). Estuarine response to a freshwater pulse. *Es-*
632 *tuarine, Coastal and Shelf Science*, *26*(6), 657–667. doi: 10.1016/0272-7714(88)
633 90041-8
- 634 Liu, W.-C., Chen, W.-B., & Kuo, J.-T. (2008). Modeling residence time response
635 to freshwater discharge in a mesotidal estuary, Taiwan. *Journal of Marine Sys-*
636 *tems*, *74*(1-2), 295–314. doi: 10.1016/j.jmarsys.2008.01.001
- 637 Losada, M., Díez-Minguito, M., & Reyes-Merlo, M. (2017). Tidal-fluvial interaction
638 in the Guadalquivir River Estuary: Spatial and frequency-dependent response
639 of currents and water levels. *Journal of Geophysical Research: Oceans*, *122*(2),
640 847–865. doi: 10.1002/2016JC011984
- 641 MacCready, P. (2004). Toward a unified theory of tidally-averaged estuarine salinity
642 structure. *Estuaries*, *27*(4), 561–570. doi: 10.1007/BF02907644
- 643 MacCready, P. (2007). Estuarine adjustment. *Journal of Physical Oceanography*,
644 *37*(8), 2133–2145. doi: 10.1175/JPO3082.1
- 645 McFarland, K., Rumbold, D., Loh, A. N., Haynes, L., Tolley, S. G., Gorman, P.,
646 ... Doering, P. H. (2022). Effects of freshwater release on oyster reef den-
647 sity, reproduction, and disease in a highly modified estuary. *Environmental*
648 *monitoring and assessment*, *194*(2), 1–30. doi: 10.1007/s10661-021-09489-x
- 649 Monismith, S. (2017). An integral model of unsteady salinity intrusion in estuar-
650 ies. *Journal of Hydraulic Research*, *55*(3), 392–408. doi: 10.1080/00221686
651 .2016.1274682
- 652 Monismith, S., Kimmerer, W., Burau, J., & Stacey, M. (2002). Structure and
653 flow-induced variability of the subtidal salinity field in northern San Fran-
654 cisco Bay. *Journal of physical Oceanography*, *32*(11), 3003–3019. doi:

- 655 10.1175/1520-0485(2002)032<3003:SAFIVO>2.0.CO;2
- 656 Navarro, G., Gutiérrez, F. J., Díez-Minguito, M., Losada, M. A., & Ruiz, J.
657 (2011). Temporal and spatial variability in the Guadalquivir Estuary: a
658 challenge for real-time telemetry. *Ocean Dynamics*, *61*(6), 753–765. doi:
659 10.1007/s10236-011-0379-6
- 660 Navarro, G., Huertas, I. E., Costas, E., Flecha, S., Díez-Minguito, M., Caballero, I.,
661 ... Ruiz, J. (2012). Use of a real-time remote monitoring network (RTRM)
662 to characterize the Guadalquivir Estuary (Spain). *Sensors*, *12*(2), 1398–1421.
663 doi: 10.3390/s120201398
- 664 Paerl, H. W., Valdes, L. M., Joyner, A. R., Peierls, B. L., Piehler, M. F., Riggs,
665 S. R., ... Ramus, J. S. (2006). Ecological response to hurricane events in the
666 Pamlico Sound system, North Carolina, and implications for assessment and
667 management in a regime of increased frequency. *Estuaries and Coasts*, *29*(6),
668 1033–1045. doi: 10.1007/BF02798666
- 669 Pritchard, D. W. (1954). A study of the salt balance in a coastal plain estuary.
670 *Journal of Marine Research*, *13*(1), 133–144.
- 671 Ralston, D. K., Geyer, W. R., & Lerczak, J. A. (2008). Subtidal salinity and veloc-
672 ity in the Hudson River estuary: Observations and modeling. *Journal of Phys-
673 ical Oceanography*, *38*(4), 753–770. doi: 10.1175/2007JPO3808.1
- 674 Tee, K.-T., & Lim, T.-H. (1987). The freshwater pulse - a numerical model with
675 application to the St. Lawrence Estuary. *Journal of Marine Research*, *45*(4),
676 871–909. doi: 10.1357/002224087788327127
- 677 Valle-Levinson, A., Wong, K.-C., & Bosley, K. T. (2002). Response of the lower
678 Chesapeake Bay to forcing from Hurricane Floyd. *Continental Shelf Research*,
679 *22*(11), 1715–1729. doi: 10.1016/S0278-4343(02)00034-1
- 680 Wang, Z. B., Winterwerp, J. C., & He, Q. (2014). Interaction between suspended
681 sediment and tidal amplification in the Guadalquivir Estuary. *Ocean Dynam-
682 ics*, *64*(10), 1487–1498. doi: 10.1007/s10236-014-0758-x